nature biomedical engineering

Patching the heart with extracellular vesicles

nature biomedical engineering

ARTICLES

https://doi.org/10.1038/s41551-018-0229-7

Cardiac recovery via extended cell-free delivery of extracellular vesicles secreted by cardiomyocytes derived from induced pluripotent stem cells

Bohao Liu[1,2,7], Benjamin W. Lee[1,3,7], Koki Nakanishi[2], Aranzazu Villasante[3], Rebecca Williamson[1,4], Jordan Metz[1,5], Jinho Kim[3], Mariko Kanai[2], Lynn Bi[3], Kristy Brown[4], Gilbert Di Paolo[4], Shunichi Homma[2], Peter A. Sims[5,6], Veli K. Topkara[2] and Gordana Vunjak-Novakovic[2,3*]

The ability of extracellular vesicles (EVs) to regulate a broad range of cellular processes has recently been exploited for the treatment of diseases. For example, EVs secreted by therapeutic cells injected into infarcted hearts can induce recovery through the delivery of cell-specific microRNAs. However, retention of the EVs and the therapeutic effects are short-lived. Here, we show that an engineered hydrogel patch capable of slowly releasing EVs secreted from cardiomyocytes (CMs) derived from induced pluripotent stem cells reduced arrhythmic burden, promoted ejection-fraction recovery, decreased CM apoptosis 24 h after infarction, and reduced infarct size and cell hypertrophy 4 weeks post-infarction when implanted onto infarcted rat hearts. We also show that EVs are enriched with cardiac-specific microRNAs known to modulate CM-specific processes. The extended delivery of EVs secreted from induced-pluripotent-stem-cell-derived CMs into the heart may help us to treat heart injury and to understand heart recovery.

The cellular secretome represents a fundamental means of intercellular communication. This complex network of proteins, lipids and nucleic acids allows for the regulation of a broad range of cellular behaviours and physiological functions[1]. Recently, the cell secretome has been used in treatments for a variety of disease states owing to its unique properties[2,3]. Extracellular vesicles (EVs) are secreted microvesicles that represent an active element of the cell secretome[4–6]. In contrast with individual secreted factors, EVs provide a unique method for cells to deliver a packaged set of bioactive components[7]. A major contributor to the activity of EVs is the collection of microRNAs (miRNAs) in their cargo[8]. These miRNAs are critical because they can individually modulate multiple different processes, leading to pleiotropic effects[9]. Importantly, EVs from different cell types or cells in different states can carry vastly different sets of miRNAs, leading to a variety of effects[7,10]. Recent research efforts have focused on leveraging EVs as a powerful therapeutic tool.

In the treatment of heart disease, standard therapies fail to recover the injured myocardium, and do not alleviate the need for heart transplantation. Stem cell therapies of the heart have demonstrated only modest improvements in ejection fraction and clinical outcomes[11–13]. While the primary use of stem cells has been to form de novo CMs[14], their ability to improve cardiac function, despite poor retention[15], has led to the discovery that implanted stem cells exert their clinical benefit largely via their secretome[12,16,17]. In particular, EVs secreted from cardiospheres or embryonic stem cells injected into infarcted hearts have been shown to attenuate ischaemic injury in both small and large animal models[18–21]. Injected EVs are thought to directly signal to the myocardium and supporting cells, including fibroblasts and endothelial cells, altering their responses to ischaemic injury. However, published studies have only used EVs from undifferentiated or partially differentiated cells, which may lack the distinct miRNAs important in cardiac-specific processes. Furthermore, similar to the key limitation of cell-based therapies, EV-based therapies of the heart have relied on injections that result in short-lived retention of the EVs. To date, no EV retention greater than 3 h post-myocardial injection[18] has been documented.

Induced-pluripotent-stem-cell-derived CMs (iCMs) offer a virtually unlimited supply of beating human CMs. Already, there has been some success in the direct application of iCMs onto the injured myocardium, including in non-human primates[22]. The clinical utility of iCMs is believed to be related to cellular engraftment onto the host myocardium and remuscularization of the infarct bed[23]. However, the presence iCMs in vivo raises concerns of tumorigenicity from undifferentiated cell fractions[12,24] and arrhythmogenicity from ectopic foci of contraction[25–27]. Previous studies using rodent neonatal CMs have demonstrated that, similar to other cell types including stem cells, CMs have an active secretome and can generate an abundance of EVs capable of regulating the phenotype of many target cells, including fibroblasts, endothelial cells and other CMs[10,28–31]. CM EVs may be packaged with miRNAs with specific activity on the heart and cardiac processes. Therefore, the secretome of iCMs may contribute to their clinical effects, but has been neither characterized nor used therapeutically.

We hypothesized that iCMs, unlike naive induced pluripotent stem (iPS) cells, secrete EVs carrying CM-specific cargo that can target the myocardium both by providing protection from injury and by promoting recovery after injury (Fig. 1). We also hypothesized that hydrogel encapsulation will allow for the sustained

[1]College of Physicians and Surgeons, Columbia University, New York, NY, USA. [2]Department of Medicine, Columbia University, New York, NY, USA. [3]Department of Biomedical Engineering, Columbia University, New York, NY, USA. [4]Department of Pathology and Cell Biology, Columbia University, New York, NY, USA. [5]Department of Systems Biology, Columbia University, New York, NY, USA. [6]Department of Biochemistry and Molecular Biophysics, Columbia University, New York, NY, USA. [7]These authors contributed equally: Bohao Liu, Benjamin W. Lee. *e-mail: gv2131@columbia.edu

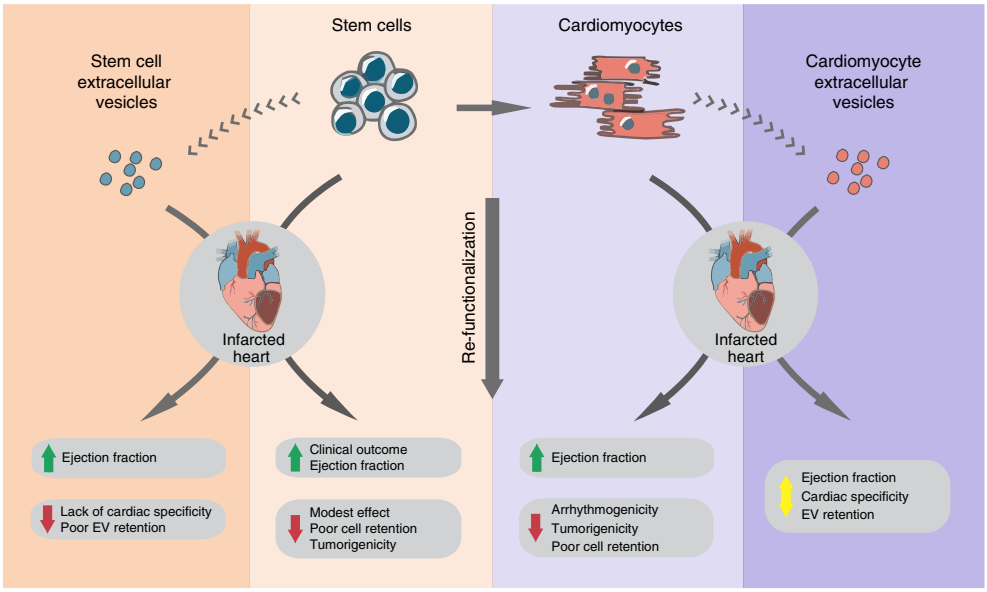

Fig. 1 | Therapeutic potential and challenges of cell- and EV-based therapies. Cell-based therapies using either stem cells or differentiated CMs have shown clinical utility in their ability to refunctionalize the injured heart. When directly injected into the heart, both stem cells and CMs have resulted in the refunctionalization of the heart and improved clinical outcomes[11–13]. However, many challenges arise from the use of cell therapies. Specifically, stem cell therapies only demonstrate modest effects, whereas CM therapies have a high propensity to induce arrhythmias[22,26,27]. Stem cell EVs have also been able to refunctionalize the injured heart, mediating the regeneration of the heart after myocardial infarction[12,16,19,20]. However, the cargo of stem cell EVs is not specific to cardiac processes. We hypothesize that iCMs, unlike naive iPS cells, secrete EVs carrying CM-specific cargo that can target the myocardium, providing protection from injury and promoting recovery after myocardial infarction.

delivery of iCM-EVs in the post-infarct environment, promoting their therapeutic effects. To this end, we developed a system that can sustainably deliver EVs to the post-infarct environment. Our results demonstrate that EVs isolated from iCMs contain a distinct set of miRNAs enriched for those known to modulate CM-specific processes. When encapsulated into an extended-release hydrogel patch capable of delivering EVs directly to an infarcted rat heart, iCM-EVs resulted in recovered ejection fraction, reduced infarct size, a decreased number of arrhythmias and prevented CM hypertrophy. Overall, the extended delivery of iCM-EVs attenuated injury and promoted recovery of the heart after ischaemic insult, suggesting that iCM-EVs may represent a cell-free system for understanding heart recovery and treating heart injury.

Results

iCMs secrete functional EVs. Secreted microvesicles were isolated from iCMs and their parent iPS cells. Nanoparticle tracking analysis and visualization by transmission electron microscopy revealed that vesicles secreted by iCMs and iPS cells were comparable in yield and size, displaying typical EV morphology and size distributions[32–35] (Fig. 2a–c). Immunoblots confirmed the presence of the EV marker tumour susceptibility gene 101 (TSG101) in isolated iCM microvesicles and the absence of the cell-specific markers golgin A2 (GM130) and Ras-related protein 5 (Rab5)[4] (Fig. 2d and Supplementary Fig. 7). Bioanalyser analysis demonstrated distinct 18S and 28S ribosomal RNA peaks exclusively in iCM RNA and not in isolated iCM-EV RNA, further verifying the successful isolation of EVs without cellular contamination (Fig. 2e).

To determine the ability of iCM-EVs to convey biological messages, we first confirmed the uptake of iCM-EVs by cardiac and vascular cells. iCMs and human umbilical vein endothelial cells (HUVECs) were cultured with iCM-EVs labelled with the non-specific membrane dye DiI. Fluorescence imaging revealed EVs within both cell types (Supplementary Fig. 1a,b). Furthermore, there was reduced iCM-EV uptake with the inhibition of dynamin-mediated endocytosis with dynasore, but not with the inhibition of micropinocytosis with ethylisopropyl amiloride (Supplementary Fig. 1c,d).

iCM-EVs have greater therapeutic potential than iPS-EVs in vitro. To compare the therapeutic potential of iPS-EVs and iCM-EVs, we tested their abilities to protect iCMs in an in vitro culture model of myocardial hypoxia. Under normoxic conditions, iCMs exhibited spontaneous rhythmic contractions that became irregular after 48 h of hypoxia (Fig. 2f). Interestingly, both iPS-EVs and iCM-EVs protected iCMs when added during hypoxia, reducing the range and variance of instantaneous beating frequencies. However, only iCM-EV treatment completely ameliorated the hypoxia-induced phenotype (Fig. 2g,h). Furthermore, iCM-EVs protected vascular cells, promoting vascular network formation during hypoxic culture (Supplementary Fig. 2). Together, these results show that while both iCMs and iPS cells secrete functionally active EVs, iCM-EVs have a greater protective effect on hypoxia-stressed iCMs.

iCM-EVs are enriched in cardiac-specific miRNAs. To characterize in detail the miRNA cargo of EVs, we performed next-generation miRNA sequencing of iPS-EVs and iCM-EVs. The sequencing results identified over 300 miRNAs with counts greater than 1 tag per million (TPM) across both groups (Supplementary Table 1). Dimension reduction using principal component analysis (PCA) was used to explore the broad miRNA differences between iPS-EVs and iCM-EVs. This unbiased approach detected two different EV populations clearly separating iPS-EVs and iCM-EVs (Fig. 3a).

Next, we used DESeq2 to identify differentially expressed miRNAs between iPS-EVs and iCM-EVs[36]. A total of 219 miRNAs were identified to be significantly differentially expressed, with false discovery rate values less than 0.05 (Supplementary Table 2). The expression levels of the subset of differentially expressed miRNAs were

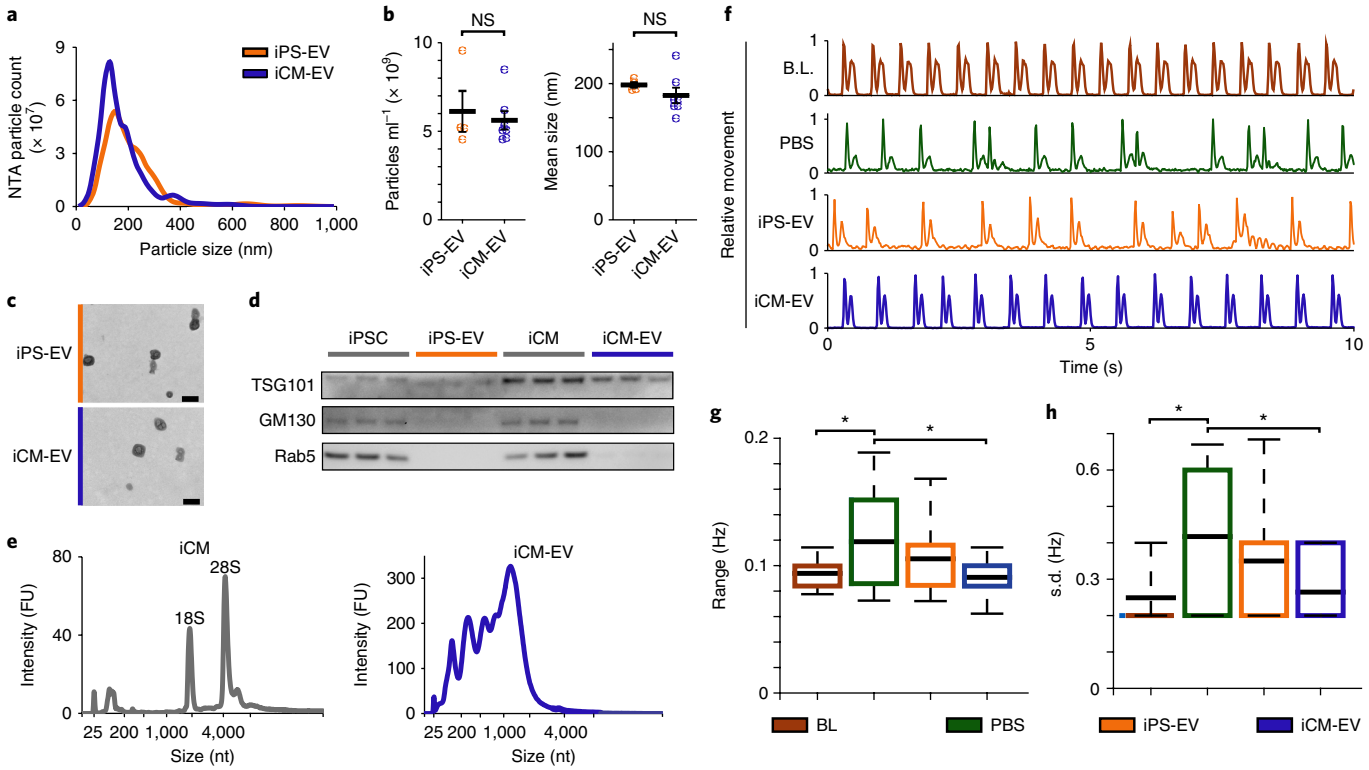

Fig. 2 | iCMs secrete functional EVs. a, Representative size distribution of microvesicles isolated from iPS cells and iCMs. NTA, nanoparticle tracking analysis. **b**, Total number and size of microvesicles (mean ± s.e.m., $n = 4$ and 8 biologically independent samples for the iPS cell and iCM groups, respectively). NS, not significant. **c**, Representative transmission electron micrographs of microvesicles (scale bars: 100 nm; experiments were repeated with similar results). **d**, Immunoblots of cell lysates and microvesicle fractions for the exosome marker TSG101 and intracellular proteins (GM130 and Rab5) ($n = 3$ biologically independent samples per group). **e**, Representative bioanalyser plots of total RNA profiles of iCMs and iCM-EVs ($n = 3$ biologically independent samples per group). FU, fluorescence units. **f**, Representative traces of spontaneously beating iCMs at baseline (BL; normoxia), and after 48 h of hypoxia with PBS (control), iPS-EVs or iCM-EVs (experiments were repeated with similar results). **g**,**h**, Range (**g**) and s.d. (**h**) of the distributions of instantaneous beating frequencies. Boxes show the mean and twenty-fifth and seventy-fifth percentiles. Whiskers show the ninth to ninety-first percentiles ($n = 49$, 35, 12 and 31 biologically independent samples for the BL, PBS, iPS-EV and iCM-EV groups, respectively). $^*P < 0.05$ by two-sided t-test.

confirmed via quantitative real-time PCR (Supplementary Fig. 3). Remarkably, we noted that the cardiac-specific miR-1 was highly abundant in iCM-EVs but nearly absent in iPS-EVs[37]. In contrast, the early embryogenesis-specific miR-302a was highly abundant in iPS-EVs and significantly decreased in iCM-EVs[38] (Table 1). A volcano plot of differentially expressed genes demonstrates asymmetric enrichment of specific miRNAs in iCM-EVs, reflecting the increased miRNA diversity in iCM-EVs (Fig. 3b). Interestingly, many of these miRNAs, including miR-1 and miR133a, are known to have significant impacts on cardiac function[39].

To predict cellular processes affected by iCM-EVs, we used miRSearch[40,41] to map the targets of a subset of miRNAs that were significantly differentially expressed and highly abundant in iCM-EVs (Fig. 3c, grey shaded area). A total of 2,357 genes were identified as targets (Supplementary Table 3). We applied gene ontology analysis to this gene set to identify significantly enriched biological processes[42,43], and detected 172 processes that were significantly enriched (Supplementary Table 4). Surprisingly, 55% of the top 20 significantly enriched biological processes (ranked by fold change) are known to be heavily involved in cardiac biology (Fig. 3d). Furthermore, the top two biological processes are those involved in the positive regulation of muscle hypertrophy. As miRNAs typically repress target function, this finding suggests that a main effect of iCM-EVs may be the repression of cardiac hypertrophy. Taken together, these results reveal that iCM-EVs contain cargo enriched in cardiac-specific miRNAs that may target the hypertrophic process.

Hydrogel patch sustainably released encapsulated EVs in a rat model of acute myocardial infarction. To investigate the effects of iCM-EV treatment on heart injury and recovery, we developed a hydrogel patch capable of sustained delivery of EVs, by encapsulating approximately 3×10^{10} iCM-EVs into a 7-mm-diameter collagen gelfoam mesh. A collagen-based hydrogel was selected because it is a well-defined neutral material with documented use in sustained delivery[44]. Quantification of the release profile using NanoSight showed that the patch could sustainably release 3×10^{10} EVs over the course of 21 days in vitro (Fig. 4a). To confirm sustained release in vivo, we labelled the iCM-EVs with the membrane dye DiI, encapsulated them into a hydrogel patch and applied them directly onto the rat myocardium. Next, we imaged explanted patches using a custom laser light sheet illumination platform (Supplementary Fig. 4a,b). At day 4 after implantation, signal intensity was reduced compared with day 0, yet indicated that a significant proportion of labelled EVs remained. By day 7 after implantation, signal intensity had markedly decreased, but remained detectable. These in vivo findings are consistent with the release profile observed in vitro (Fig. 4b).

After confirming delivery of the iCM-EVs, we designed a rat model of myocardial infarction by left anterior descending artery (LAD) ligation to analyse the effects of iCM-EV treatment (Fig. 4c). Athymic nude rats were used to remove any possible immune-mediated interactions. Patches containing iPS-EVs, iCM-EVs or phosphate buffered saline (PBS) were applied directly onto the rat myocardium immediately following LAD ligation. The PBS patch group was included to isolate the effects of the EV treatments from

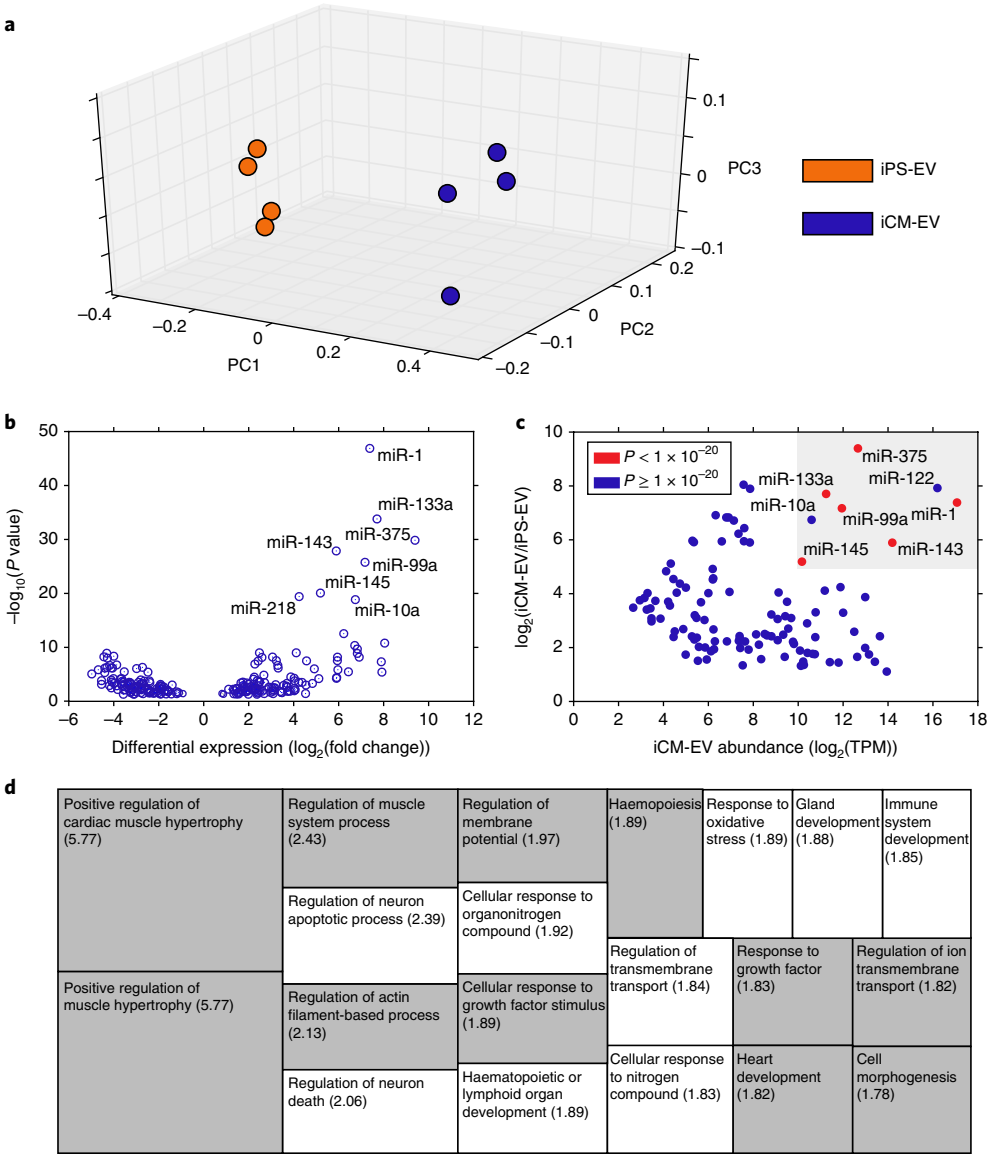

Fig. 3 | iCM-EVs are enriched in cardiac-specific miRNAs. a, PCA of iPS-EV and iCM-EV miRNA expression ($n=4$ biologically independent samples per group). **b**, Volcano plot of significantly differentially expressed miRNAs. *P* values calculated via Wald test and adjusted using the Benjamini–Hochberg method ($n=4$ biologically independent samples per group). **c**, Differentially expressed and abundantly expressed miRNAs in iCM-EVs. The grey shaded region contains miRNAs used in subsequent gene ontology analysis ($n=4$ biologically independent samples per group). **d**, Top 20 significantly enriched biological processes with the highest fold changes. Fold change over expected enrichment values are shown in parenthesis. Cardiac-related processes are shaded grey.

the effects of the collagen patch. Rats treated with sustained-delivery patches were compared with sham rats that received thoracotomy but no ligation or patch and rats that received ligation but no patch (that is, the no-treatment group). Telemetry devices were implanted for telemetric monitoring of arrhythmia during the first seven days after LAD ligation. Echocardiography was performed at two and four weeks, and the histological analysis was performed at the four week endpoint.

To demonstrate that EVs deliver cargo to the myocardium in vivo, we labelled the iCM-EVs with the cell membrane linker PKH-67 and incorporated them into a patch for implantation. Fluorescent imaging of frozen sections of the rat hearts 24 h after implantation revealed the presence of labelled EVs in the myocardium (Supplementary Fig. 4c–e). Next, we quantified the levels of EV-derived miRNAs in the rat myocardium and demonstrated that rat hearts treated with EV patches had significantly increased levels of miRNAs present in high quantities in EVs (Supplementary Fig. 4f). Together, these results suggest that EVs deliver their miRNA cargo when released from a patch implanted on the myocardium.

iCM-EVs are not arrhythmogenic and promote recovery of contractile function. To determine whether EVs are arrhythmogenic, we conducted continuous electrocardiogram monitoring during the first five days after infarction. All LAD ligation groups showed classic electrocardiogram waveform progression following myocardial infarction. LAD ligation resulted in arrhythmic events including atrioventricular block, premature ventricular contraction, ventricular tachycardia and ventricular fibrillation (Fig. 5a). A significant difference was noted in the cumulative arrhythmic burden (total number of events) within the first five days between the sham and all LAD ligation groups, but not between iCM-EV or iPS-EV and the control groups (Fig. 5b and Supplementary Fig. 5a). Rats were then stressed with isoproterenol, which is known to cause ventricular arrhythmias, seven days after surgery. Quantification of the

Table 1 Fold change and expression levels (TPM) of the most abundant miRNAs in iCM-EVs that are differentially expressed

miR	$\log_2$(fold change)	iPS-EV (TPM)	iCM-EV (TPM)
miR-1	7.38	590	137,765
miR-302a-5p	−2.52	371,799	81,598
miR-122-5p	7.92	49	75,250
miR-92a-3p	−1.60	56,168	24,093
miR-143-3p	5.89	213	18,692
miR-302b-3p	−3.31	146,633	18,151
miR-30d-5p	1.11	5,538	15,753
miR-27b-3p	2.42	1,819	12,754
miR-99b-5p	1.47	2,940	10,924
miR-200b-3p	1.75	2,134	9,108

total arrhythmic burden following isoproterenol challenge revealed that the animals treated with patches containing EVs, and in particular those containing iCM-EVs, experienced significantly fewer arrhythmic events than those treated with PBS patches without EVs. Interestingly, animals treated by PBS patch showed significantly more arrhythmic events than infarcted animals that did not receive a patch (Fig. 5c and Supplementary Fig. 5b). These results indicate that EV treatment did not increase the arrhythmia burden of rats.

Echocardiograms were performed two and four weeks after LAD ligation. At two weeks, compared with sham rats, all LAD-ligated rats showed significantly increased diastolic and systolic diameters as well as decreased ejection fractions (Fig. 5d and Supplementary Table 5). These measurements are consistent with cardiac dilation and reduced cardiac function following injury. Interestingly, even at the two week time point the iCM-EV-patch-treated group showed reduced cardiac dilation and better function with higher ejection fraction compared with the iPS-EV patch, PBS patch and no-patch control groups. By four weeks, animals treated with iCM-EV patches no longer exhibited significant differences in any of the measured echocardiogram parameters compared with sham animals. Additionally, iCM-EV-patch-treated animals showed significantly improved parameters compared with untreated control animals with myocardial infarction (Fig. 5e and Supplementary Table 5). In M-mode echocardiography, anterior wall motion was severely blunted in the untreated rats with myocardial infarction and patch-treated-control rats, but retained greater motion in animals treated with iCM-EV patches (Fig. 5f). Notably, neither iPS-EV- nor PBS-patch-treated animals demonstrated a recovery of function at four weeks. Collectively, these results show that iCM-EVs protect hearts from declining myocardial function following LAD ligation, and recover near-normal function by four weeks.

EV-treated hearts have a reduced infarct size and reduced pathological hypertrophy. Four weeks after LAD ligation and patch placement, the effects of iCM-EVs on the heart's response to injury

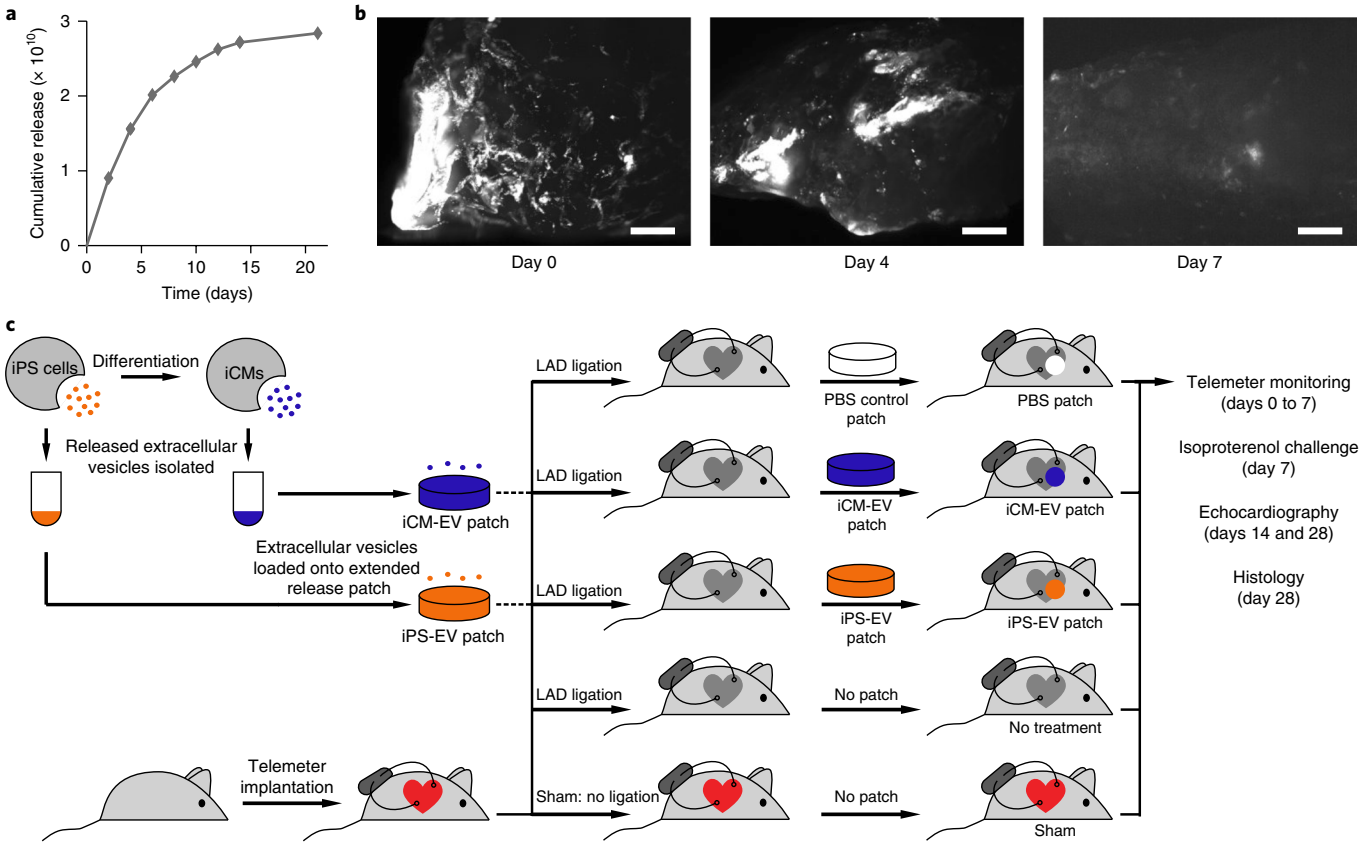

Fig. 4 | Hydrogel patch sustainably released encapsulated EVs in a rat heart infarction model. a, Cumulative release profile of EV-containing patches over 21 days in vitro, as quantified by NanoSight ($n = 2$ biologically independent samples). **b**, Representative images of DiI-stained EVs present in hydrogel patches explanted 0, 4 and 7 days after implant onto rat myocardium ($n = 1$ biologically independent sample per day). Scale bars: 200 μm. **c**, Schematic of the experimental set-up for the rat model: EVs were isolated from iPS cells or iCMs and incorporated into a patch as therapy in a rat acute myocardial infarction model.

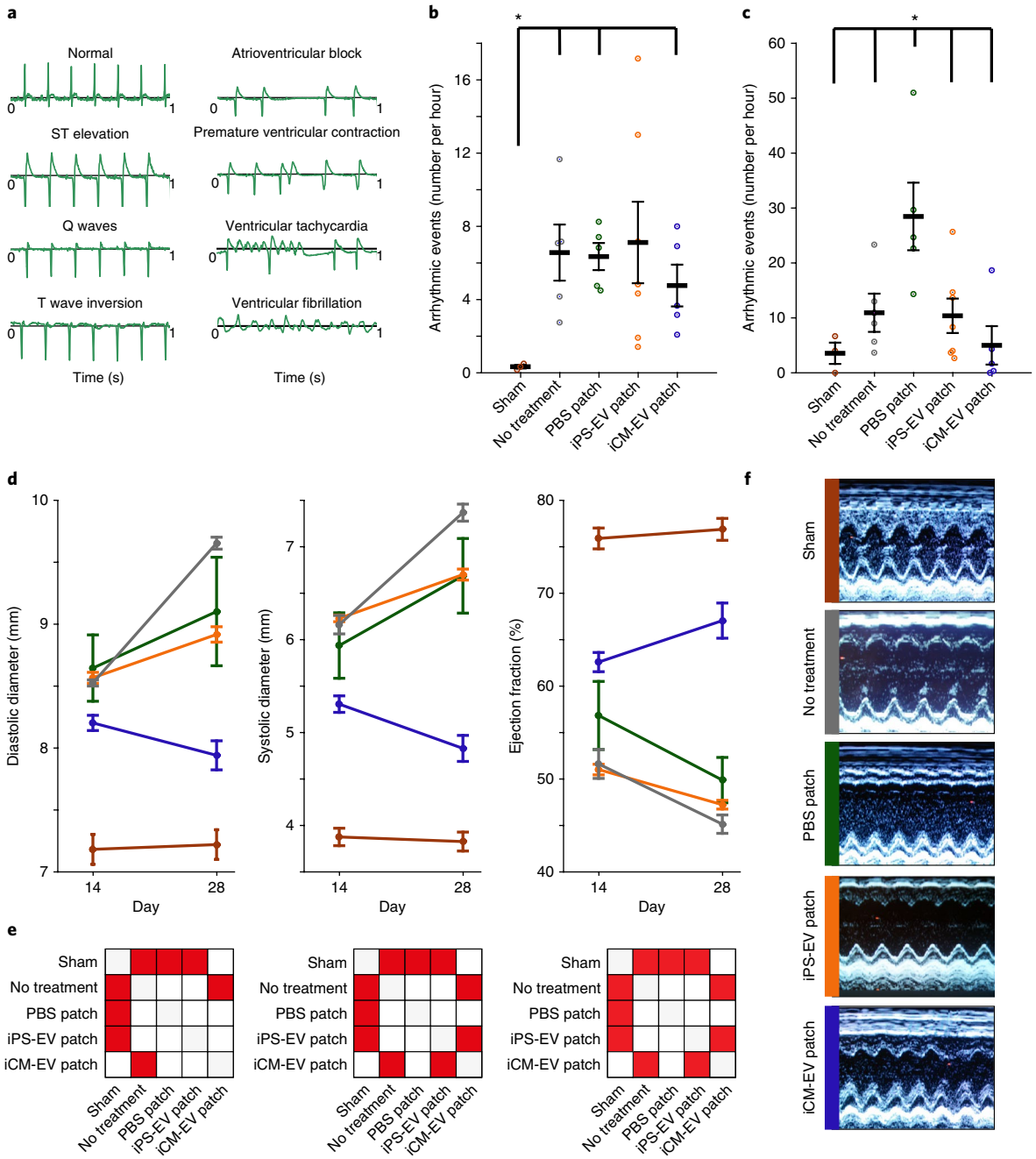

Fig. 5 | iCM-EVs are non-arrhythmogenic and promote recovery of heart contractile function. a, Electrocardiogram progression after LAD. All rats exhibited ST elevations following LAD ligation, followed by Q waves and T wave inversion within three days. LAD ligation resulted in arrhythmic events including atrioventricular block (characterized by a P wave without a subsequent QRS complex), premature ventricular contraction (characterized by a widened QRS complex without a preceding P wave), ventricular tachycardia (characterized by more than three consecutive QRS complexes without preceding P waves) and ventricular fibrillation (characterized by uncoordinated electrical activity). **b**, Number of arrhythmic events per hour experienced by animals during the first 5 days after infarction (mean ± s.e.m., $n = 3$, 5, 5, 7 and 6 biologically independent samples for the sham, no-treatment, PBS patch, iPS-EV patch and iCM-EV patch groups, respectively). *$P < 0.05$ by two-sided t-test. **c**, Number of arrhythmic events per hour experienced by animals for 3 h after isoproterenol challenge (mean ± s.e.m., $n = 3$, 5, 5, 7 and 5 biologically independent samples for the sham, no-treatment, PBS patch, iPS-EV patch and iCM-EV patch groups, respectively). *$P < 0.05$ by two-sided t-test. **d**, Quantified echocardiogram parameters of animals at the 2 and 4 week time points (mean ± s.e.m., $n = 5$, 4, 6, 7 and 6 biologically independent samples for the sham, no-treatment, PBS patch, iPS-EV patch and iCM-EV patch groups, respectively). **e**, Statistical significance of the quantified echocardiogram parameters in **d** between all groups at four weeks, quantified by a two-tailed t-test. Red indicates a significant difference with Bonferroni-corrected $P < 0.05$. **f**, Representative M-mode echocardiographs at 4 weeks ($n = 6$, 5, 6, 7 and 6 experimental repetitions in different animals for the sham, no-treatment, PBS patch, iPS-EV patch and iCM-EV patch groups, respectively, with similar results).

were examined histologically. Movat's pentachrome staining was used to visualize the myocardium (Fig. 6a,b). Total infarct size, as measured by the percentage of fibrosis in the left ventricle, was significantly smaller in iCM-EV-patch-treated animals than untreated and PBS-patch-treated animals (Fig. 6c). Importantly, iPS-EV-patch-treated animals demonstrated a modest but non-sig-

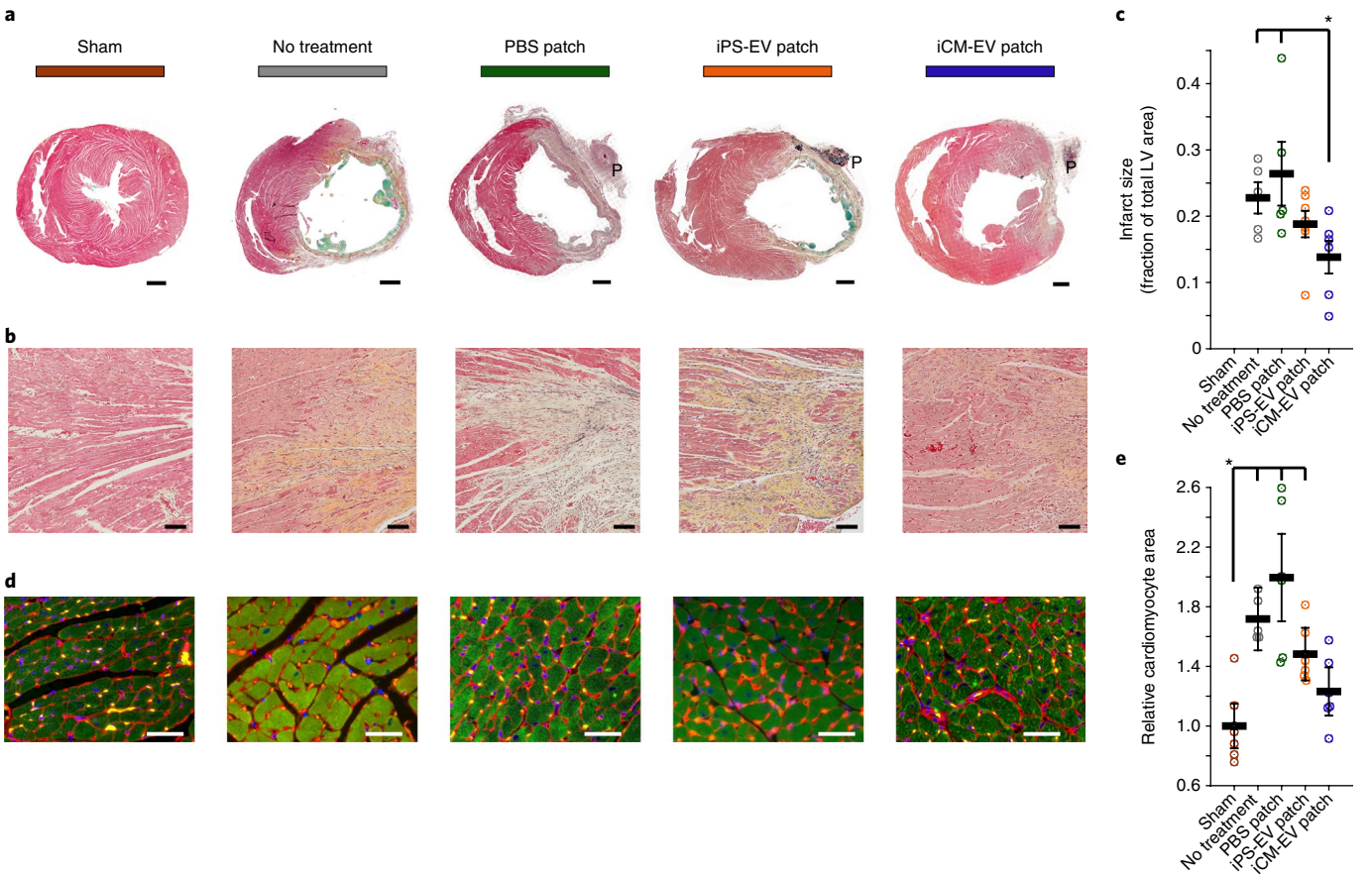

Fig. 6 | iCM-EV-treatment-reduced infarct size and CM hypertrophy. a, Representative transverse cardiac sections stained with Movat's pentachrome stain (scale bars: 1 mm). The letter P indicates the location of the patch. **b**, High-power images of the infarct border zone (scale bars: 100 μm) (experiments were repeated in $n = 5$, 5, 7 and 6 biologically independent samples for the no-treatment, PBS patch, iPS-EV patch and iCM-EV patch groups, respectively, with similar results). **c**, Infarct size as a percentage of the total left ventricle (LV) area (mean ± s.e.m., $n = 5$, 5, 7 and 6 biologically independent samples for the no-treatment, PBS patch, iPS-EV patch and iCM-EV patch groups, respectively). $^*P < 0.05$ by two-tailed *t*-test. **d**, Sections were stained with wheat-germ agglutinin (red), for troponin (green) and with DAPI (blue). Scale bars: 50 μm. **e**, Relative CM area quantified (mean ± s.e.m., $n = 6$, 5, 6, 6 and 6 biologically independent samples for the sham, no-treatment, PBS patch, iPS-EV patch and iCM-EV patch groups, respectively, with similar results). $^*P < 0.05$ by two-tailed *t*-test.

nificant difference in infarct size compared with untreated and PBS-patch-treated animals. As sequencing analysis suggested a specific effect of iCM-EVs on hypertrophy, we quantified rat CM sizes at the four week time point. Wheat germ agglutinin staining revealed that CM size was significantly smaller in iCM-EV-treated hearts compared with all other LAD ligation groups (Fig. 6d,e). These results suggest that iCM-EV treatment after LAD ligation was able to prevent the expansion of the infarct area and reduce pathological hypertrophy. Finally, we performed a correlation analysis to determine the interdependence of measured endpoints, including total infarct size, isoproterenol-induced arrhythmias, cell size and ejection fraction. A significant positive correlation was noted between cell size and total infarct size, whereas a significant negative correlation was noted between ejection fraction and both total infarct size and cell size (Supplementary Table 6).

EV-treated hearts have reduced apoptosis. iCM-EV-treated hearts at 4 weeks post-implant did not demonstrate significant increases in infarct size compared with hearts at 24 h after LAD ligation, in contrast with all other LAD ligation groups (Supplementary Fig. 6). Therefore, we hypothesized that iCM-EVs may be exerting their therapeutic effect early in the injury process and examined the function of the heart 24 h after LAD ligation in the iCM-EV patch, iPS-EV patch and no-treatment-of-myocardial-infarction groups (Fig. 7a). Interestingly, iCM-EV-patch-treated animals had greater preserved ejection fractions than either iPS-EV-patch-treated or untreated animals, suggesting that iCM-EVs may exert their protective effects within the first 24 h. To determine whether this effect may have been mediated by a reduction in ischaemia-induced apoptosis, we tested the ability of both iPS-EVs and iCM-EVs to reduce apoptosis in an in vitro model of CM ischaemia. CMs were treated with PBS, iPS-EVs or iCM-EVs and subsequently subjected to 1% oxygen in a hypoxic chamber for 24 h. Quantification of apoptosis using activated caspase-3 demonstrated that iCM-EVs were able to significantly reduce apoptosis in hypoxic CMs (Fig. 7b,c). Next, we examined the amount of apoptosis in iCM-EV-treated rat hearts or untreated rat hearts at 24 h after LAD ligation. Terminal deoxynucleotidyl transferase dUTP nick-end labelling (TUNEL) staining showed that rats treated with iCM-EV patches had significantly decreased areas of apoptotic cells (Fig. 7d,e). Together, these results suggest that one of the therapeutic mechanisms of iCM-EVs is their ability to prevent hypoxia-induced apoptosis in newly infarcted hearts.

Discussion

Here, we document that the extended delivery of human iCM-EVs from a hydrogel patch protects the acutely injured heart from pathological hypertrophy and leads to functional recovery. The use of iCM-EVs thus represents a promising cell-free alter-

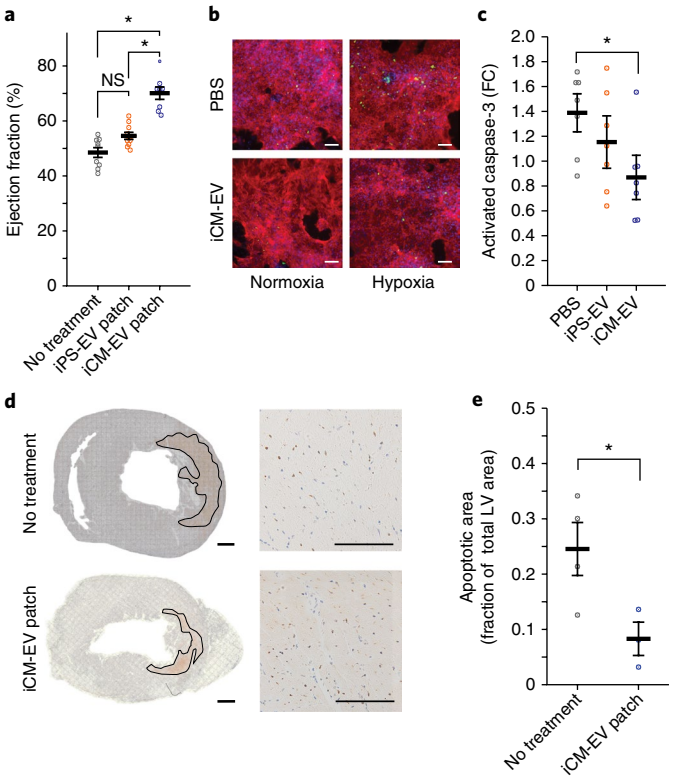

Fig. 7 | iCM-EV treatment prevents apoptosis in the acutely infarcted heart. a, Quantification of ejection fraction 24 h after LAD ligation (mean ± s.e.m., $n = 9$, 10 and 8 biologically independent samples for the no-treatment, iPS-EV patch and iCM-EV patch groups, respectively). $^*P < 0.05$ by two-tailed t-test. **b**, CMs stained with activated caspase-3 (green), troponin (red) and DAPI (blue) subjected to either hypoxia or normoxia and treated with either iCM-EVs or PBS. Scale bars: 100 µm. **c**, Quantification of the numbers of caspase-3-positive hypoxic CMs relative to normoxic CMs (mean ± s.e.m., $n = 7$ biologically independent samples per group). $^*P < 0.05$ by two-tailed t-test. FC, fold change. **d**, Representative transverse cardiac sections stained with TUNEL (left; scale bars: 1 mm) and at high magnification (right; scale bars: 100 µm). **e**, Quantification of the apoptotic area as a fraction of the total left ventricular (LV) area (mean ± s.e.m., $n = 4$ and 3 biologically independent samples for the no-treatment and iCM-EV patch groups, respectively). $^*P < 0.05$ by two-tailed t-test.

native for cardiac recovery. As EVs carry cargo representative of their origin cells, the choice of cell type is crucial in determining the therapeutic potential of secreted EVs. In this study, we demonstrate significant differences in the miRNA cargo of EVs isolated from iPS cells versus terminally differentiated CMs. We show that iCM-EVs are enriched in miRNAs that modulate cardiac-specific processes. Previous studies have implicated the ability of pluripotent stem cell EVs to affect the heart through the delivery of stem-cell-specific miRNAs[19,38]. However, stem cell EVs may not have cell-type-specific effects. We show that iCM-EVs clearly provide more therapeutic benefit after injury than iPS-EVs when released from an extended delivery patch. iCM-EVs had greater effects on reducing infarct size, hypertrophy and apoptosis compared with iPS-EVs. iCM-EVs were able to affect the injured heart through more CM-specific pathways, including pathological hypertrophy. Although additional studies will be needed to elucidate the detailed mechanisms of the individual components of iCM-EV cargo, we believe that the extended delivery of cell-type-specific EVs represents a promising advancement in EV-based therapies of the heart.

In this study, we used iPS-cell-derived CMs as a source of therapeutic EVs. iPS cells and their cardiac derivatives are powerful cell sources for cardiac regeneration. While previous work has highlighted the benefits of EVs derived from non-human cells, our study demonstrates the therapeutic effectiveness of EVs from human iPS-cell-derived CMs. Human iPS cells offer a flexible platform to refine EV-based therapeutics. The continued improvements in differentiation[45] and maturation[46] of these cells may result in the generation of EVs with greater therapeutic potential and cardiac specificity. iPS cells are amenable to gene editing while preserving their ability to differentiate[47], allowing for the isolation of genetically modified EVs. Such a system provides the opportunity to precisely control the contents that EVs deliver. A unique property of EVs is their ability to deliver multiple miRNAs acting synergistically on separate processes to produce therapeutic effects. Thus, the ability to tailor the miRNA profiles of iCM-EVs will allow optimization of their therapeutic benefits.

One of the limitations of the use of iCMs in the injured myocardium is the concern over arrhythmogenicity due to ectopic foci of contraction or poor engraftment onto the host myocardium[25,48]. We have discovered that iCM-EVs, in contrast with their cellular counterparts, do not induce arrhythmias as observed following implantation of stem-cell-derived CMs into primate hearts[22]. Most importantly, EVs exert many of the same effects as CM cell therapy, including recovery of ejection fraction, reduction of fibrosis and prevention of cellular hypertrophy. EVs are easy to isolate and stable frozen over long periods of time, presenting an opportunity for off-the-shelf products that can be used in the acute setting as opposed to cells that can take months to isolate and grow. Furthermore, cell therapies can often induce unwanted host immunogenic responses and, although we did not study the immunogenicity of EVs in our model, recent studies have suggested that EVs have low immunogenicity[49]. Therefore, from a process-oriented standpoint, EV-based cell-free therapies have the potential to bypass many of the hurdles of direct cell therapies. In particular, iCM-EVs represent an alternative to cell therapy that may be safe and practical to implement in a clinically relevant setting.

We developed and implemented an EV encapsulation method that retains EVs in the infarct environment. While a variety of methods have been suggested for delivering cells or EVs into the heart, common techniques such as single-bolus injections often result in minimal concentrations of therapeutic product in the injured area, with up to 90% of cells dying or washing away in cell injections[50]. Analysis of EV retention following injection has only been completed for up to 3 h post-injection and has shown significant decreases in EV content[18]. Encapsulation of EVs within a natural extracellular matrix patch prevents washout and maintains local concentrations of EVs. We show that the release of EVs from the patch over the course of weeks allows for continuous and direct treatment of the infarct area through the acute and subacute phases of myocardial infarction and recovery. While injections are less invasive than patch placement, hydrogels can now be delivered into the heart by percutaneous approaches[51,52], and we envision that these strategies are applicable to EV patch deliveries.

In summary, we have shown that the extended delivery of iCM-EVs can protect and promote recovery of the heart. Although more work is required to completely elucidate the mechanisms of iCM-EV function, EVs from iCMs represent a promising new direction for understanding heart recovery and treating heart injury.

Methods

Cell culture and CM differentiation. Human pluripotent stem cells were cultured and differentiated based on previously published protocols. iPS cells (C2A line, kindly provided and previously authenticated[53] by S. Duncan through a material transfer agreement) were cultured on 1:80 diluted growth-factor-reduced Matrigel (Corning) in mTeSR-1 (Stemcell Technologies) supplemented with 1% penicillin/streptomycin (Thermo Fisher Scientific) at 37 °C and 21% O_2. iPS cells were

passaged at 80–90% confluence using 0.5 mM EDTA (Thermo Fisher Scientific) and cultured for 24 h in iPS medium supplemented with 5 μM Y-27632 (Tocris Bioscience) before maintenance in iPS medium. Cells were used between passages 40 and 70. Pluripotent stem cell culture was performed using serum-free medium. Stem cells were regularly tested for mycoplasma contamination.

Differentiation into CMs was performed using a stage-based protocol in RPMI-1640 (Thermo Fisher Scientific) supplemented with 0.5 mg ml^{-1} recombinant human albumin (Sigma–Aldrich), 213 μg ml^{-1} L-ascorbic acid 2-phosphate (Sigma–Aldrich) and 1% penicillin/streptomycin to produce CM medium. iPS cells were grown to 80–90% confluence and changed into CM medium supplemented with 3 μM CHIR99021 (Tocris Bioscience) for 2 days. The medium was then changed to CM medium supplemented with 2 μM Wnt-C59 (Tocris Bioscience) for 2 days before switching to CM medium without any supplements. Contracting cells were appreciated by day 9 after the start of differentiation. Experiments were performed using wells with >70% beating cells at days 9–21. CM differentiation was performed using serum-free medium.

HUVECs were isolated from discarded post-natal and fully de-identified umbilical cords under the approved Columbia University Institutional Review Board protocol IRB-AAAC4839. Cells were grown in endothelial growth medium-2 (EGM-2; Lonza) and used between passages 6 and 9.

EV isolation and NanoSight analysis of size and yield. EVs were isolated using the miRCURY Exosome Isolation Kit (Exiqon) according to the manufacturer's protocol. In brief, 50–70% confluent iPS cells or day 12–19 iPS-CMs were washed once with PBS and switched to fresh serum-free culture medium, which was collected after 48 h incubation and centrifuged at 10,000 *g* for 10 min to remove cell debris. Exosome isolation reagent (400 μl) was added per 1 ml medium and EVs were allowed to precipitate overnight. Precipitated EVs were spun at 10,000 *g* for 45 min at 4 °C and gently washed twice with phosphate buffered saline (PBS; Thermo Fisher Scientific), resulting in a clean pellet for downstream use. Isolated EVs were reconstituted in PBS for nanoparticle tracking analysis. Particle size distributions and yields of EVs were determined using NanoSight (Malvern).

Transmission electron microscopy. EV pellets, isolated as described above, were re-suspended in 4% electron-microscopy-grade paraformaldehyde in sodium phosphate buffer (Electron Microscopy Sciences). Some 10 μl of the EVs were placed on Formvar/carbon-coated electron microscopy grids (Electron Microscopy Sciences) for 20 min, after which excess solution was wicked off with filter paper. Grids were negatively stained with a uranyl–oxalate solution consisting of a 1:1 solution of 4% uranyl acetate and 0.15 M oxalic acid, adjusted to pH 7 with ammonium hydroxide (all reagents from Electron Microscopy Sciences) for 5 min. Excess stain was removed using filter paper and allowed to dry. Grids were examined using a JEOL JEM-1200 EXII transmission electron microscope. Images were captured using an ORCA-HR digital camera (Hamamatsu) and recorded with an AMT Image Capture Engine (Advanced Microscopy Techniques).

Western blots. iPS cells, iCMs and EVs isolated from these cells were washed with ice-cold PBS followed by lysis in RIPA Buffer (Thermo Fisher Scientific) supplemented with protease and phosphatase inhibitor cocktails (Roche), followed by centrifugation at 16,000 *g* for 15 min at 4 °C. Protein concentrations of both the cell lysate and EV lysate were determined using a Pierce BCA Protein Assay Kit (Thermo Fisher Scientific). For western blotting, lysates were fractionated via sodium dodecyl sulphate polyacrylamide gel electrophoresis on NuPAGE 4–12% Bis-Tris Protein Gels (Thermo Fisher Scientific) and transferred onto nitrocellulose membranes for immunoblotting.

Antibodies were used at the following concentrations: anti-TSG101 rabbit polyclonal antibody (1:1000; Abcam); anti-GM130 mouse monoclonal antibody (1:500; BD Transduction Laboratories); and anti-Rab5 mouse monoclonal antibody (1:1000; Synaptic Systems).

Quantitative PCR. Total RNA was isolated either from cells using the miRNeasy Mini Kit (Qiagen) or EV pellets using the miRCURY RNA Isolation Kit (Exiqon) according to the manufacturer's protocol. Samples were quantified using 2100 Bioanalyzer (Agilent Technologies). Complementary DNA (cDNA) from cells was made using the High-Capacity cDNA Reverse Transcription Kit (Applied Biosystems), whereas cDNA from EVs was made using the Universal cDNA Synthesis Kit (Exiqon). Quantitative PCR was performed on the StepOnePlus Real-Time PCR System (Applied Biosystems) where each well contained 4 μl diluted cDNA, 5 μl SYBR Green PCR Master Mix (Applied Biosystems) and 1 μl primers (all primers from Exiqon). Data were either analysed as cycle threshold (C_t) values or using the $\Delta\Delta C_t$ method to calculate normalized relative expression.

EV labelling and uptake by cells. Isolated and re-suspended EVs were stained with 1:100 diluted DiI (Thermo Fisher Scientific)—a non-specific membrane dye—for 15 min at room temperature. Excess dye was removed using exosome spin columns (MW 3000; Thermo Fisher Scientific) per the manufacturer's instructions.

For uptake studies, stained EVs from 1 ml medium (approximately 6×10^9 EVs) were cultured with iPS-CMs or HUVECs for 2 h at 37 °C in 2% O_2 and 5% CO_2 in the presence of either 150 μM dynasore hydrate (Sigma–Aldrich), 75 μM 5-(N-Ethyl-N-isopropyl)amiloride (Sigma–Aldrich) or an equivalent amount of dimethyl sulfoxide (Corning) as a control. Cells were then washed twice with PBS, fixed with 4% paraformaldehyde (Thermo Fisher Scientific) and stained as outlined below. The number of EVs present in the cells was quantified using ImageJ thresholding and normalized to the total number of nuclei (4′,6-diamidino-2-phenylindole (DAPI)) per field. Multiple fields were quantified in each case.

Measurements of CM contractility. iCMs at days >30 post-differentiation were cultured in hypoxia (2% O_2) for 2 days as a model of myocardial ischaemia either in the presence of a high concentration of EVs (approximately 1.2×10^{10}) or without added EVs. At baseline before hypoxia culture, or after two days of culture in hypoxia, videos were captured on an Olympus IX81 using a Pike Camera (Allied Vision Technologies) at 60 frames per second with SPLASSH software[37]. Videos were exported into MATLAB using a custom algorithm that allowed the user to measure absolute intensity changes in a user-defined area in a frame-by-frame manner. Averaging over the entire area yielded a trace representing total movement with paired peaks, where the first narrower peak represented contraction and a second shallower and wider peak represented relaxation. The resulting traces were thresholded and the times of each contraction were obtained. The instantaneous contraction frequency was then approximated by calculating the average frequency in overlapping 5 s windows. Inter-beat variation was quantified using two metrics: the frequency range, which denotes the maximum range of instantaneous frequencies calculated for each trace, and the frequency s.d., which denotes the s.d. of the instantaneous frequencies calculated for each trace.

Assessment of endothelial networks. HUVECs of passages 6–9 were seeded onto growth-factor-reduced Matrigel (Corning)-coated surfaces at a concentration of 5×10^4 cells cm^{-2} either in the presence or absence of 1.2×10^{10} EVs in hypoxia (2% O_2) as a model of ischaemia for 24 h. After 24 h, phase-contrast images were acquired using the Olympus IX81 and the Hamamatsu C4742-95 camera. Images were traced, thresholded and skeletonized using ImageJ (https://imagej.net/Welcome). The total number of branches, total number of junctions and cumulative network length were quantified for each skeleton.

Assessment of hypoxia-induced CM death. iPS-CMs at >30 days post-differentiation were cultured in hypoxia (2% O_2) for 24 h as a model of myocardial ischaemia in the presence of either a high concentration of iPS-EVs or iCM-EVs (~1.25×10^9 EVs) or without added EVs. Cells were then washed twice with PBS, fixed with 4% paraformaldehyde (Thermo Fisher Scientific) and stained as outlined below. Activated caspase-3-positive cells were quantified using ImageJ thresholding. Multiple fields were quantified for each sample.

EV miRNA sequencing. Isolated total RNA from four iPS-EV and four iCM-EV samples were sent to Exiqon for miRNA library preparation, sequencing and mapping. Eight separate miRNA profiles were generated. Raw counts were converted to TPM, then visualized by PCA along the first three principal components using the scikit-learn library in Python. Raw count tables for these samples were used as input to DESeq2 to determine differential expression of miRNAs between the iPS-EV and iCM-EV groups. The sets of predicted targets for each of the miRNAs with the greatest differential expression and abundance in iCM-EVs were determined with Exiqon's prediction algorithm, miRSearch. These targets were collectively analysed with PANTHER for gene ontology enrichment.

Patch preparation and EV-release kinetics. EV-containing patches were created via gelation of collagen within a gelfoam mesh. GELFOAM (Pfizer) was cut into 7-mm-diameter cylinders using a dermal biopsy punch (Miltex) under sterile conditions. Some 100 μl of collagen and EV solution containing 2 mg ml^{-1} of rat tail Collagen Type I (Corning) buffered to neutral pH with 10× Dulbecco's modified Eagle's medium, HEPES and 1 M sodium hydroxide (Thermo Fisher Scientific), and 3×10^{10} EVs in PBS were added to each gelfoam mesh and polymerized at 37 °C for 30 min. This resulted in approximately 10^8 EVs per gram of body weight loaded into the patch, which is in line with previous animal studies[18,54]. Patches without EVs served as a control. Patches were washed once for 30 s in PBS and used either for characterization of EV release or immediate implantation into a rat.

For the release experiment, patches were immersed in 1 ml PBS at 37 °C. PBS was replaced every 2 days for the first 14 days and one final time on day 21. Release was quantified by NanoSight as above. Laser light sheet fluorescence microscopy was used to image explanted EV patches at 0, 4 and 7 days post-implantation. The light sheet imaging system was constructed using commercially available optical parts and hardware. A thin laser sheet (thickness: ~3 μm) was created by passing the laser beam (Jive 561 nm 200 mW laser; Cobolt) through a cylindrical lens (ACY254-050-A; Thorlabs). A mirror (PF10-03-M01; Thorlabs) was placed between the laser source and the cylindrical lens to change the laser beam direction. The laser sheet was then illuminated across the heart patch that was placed onto a motorized sample stage (PT1-Z8; Thorlabs). The emission light from EVs within the patch was passed through an optical filter (FF02-641/75-25; Semrock) and a tube lens (U-TLU; Olympus) and imaged using a camera (Zyla sCMOS 4.2; Andor) with 4× (PlanN 4×, NA 0.10; Olympus), 10× (PlanN 10×, NA 0.25; Olympus) and 20× (LUCPlanFLN 20×, NA 0.45; Olympus) objective lenses.

For the in vivo uptake studies, EVs from 10 ml medium (approximately 3×10^{10} EVs) were stained with PKH-67 (Sigma–Aldrich) per the manufacturer's instructions. Excess dye was removed using exosome spin columns as previously described. Labelled EVs were incorporated into the collagen patch and implanted onto the rat myocardium. Rat hearts were then explanted for histological analysis.

Rat model of acute myocardial infarction. Animal work was performed under a protocol approved by the Columbia University Institutional Animal Care and Use Committee. Athymic nude (Hsd:RH-Foxn1^{rnu}) Sprague Dawley rats (Harlan) aged 15–19 weeks were first implanted with a bipotential telemeter (CTA-F40) capable of transmitting electrocardiogram, temperature and movement data to a paired receiver and computer (all from Data Sciences International). Rats were anaesthetized with a cocktail of 95 mg kg^{-1} ketamine and 5 mg kg^{-1} xylazine. The CTA-F40 telemeter was placed in the dorsal subcutaneous space and leads were positioned subcutaneously in a standard lead II configuration and sutured to the underlying muscle.

One week after telemeter placement, rats received a myocardial infarction by LAD ligation and subsequently implanted with a patch. Rats were anaesthetized with a cocktail of 95 mg kg^{-1} ketamine and 5 mg kg^{-1} xylazine, intubated, and mechanically ventilated on 100% O_2 with 1–5% inhaled isoflurane. The heart was exposed by left thoracotomy, the LAD was ligated using an 8–0 prolene suture (Covidien) and success of the ligation was confirmed when the anterior wall of the left ventricle turned pale. The patch was fabricated as described above, washed briefly in PBS and immediately sutured onto the myocardium using two 8–0 sutures. Electrocardiograms were monitored for at least one week and echocardiograms were recorded several times over the experimental period of one month. Rats were euthanized with CO_2 four weeks after LAD ligation, and hearts were immediately explanted, washed twice with ice-cold PBS, weighed, grossly sectioned and prepared for histological analysis.

Telemetric monitoring of cardiac function. Animals were implanted with telemetric transmitters (CTA-F40) one week before LAD ligation. Electrocardiograms were acquired continuously from one day before LAD ligation surgery until eight days after surgery using the Data Sciences International system on Ponemah 6.0 software (https://www.datasci.com/products/software/ponemah). At 7 days following LAD ligation, rats were challenged with 0.1 mg kg^{-1} isoproterenol (Sigma–Aldrich), which is known to induce ventricular arrhythmias in rats.

Raw electrocardiogram traces were viewed in Ponemah 6.0 (Data Sciences International) as follows: for five days following LAD ligation, the number of arrhythmic events (atrioventricular block, premature ventricular contraction, ventricular tachycardia or ventricular fibrillation) was counted for one minute every ten minutes. The number of arrhythmic events was also counted continuously for the three hours following isoproterenol injection. The mean event times were calculated as the mean of the mean event times for each animal.

Echocardiography. Serial echocardiography was carried out at two and four weeks after the LAD ligation and patch placement. Rats were placed under light anaesthesia (2% isoflurane) and imaged using the Sonos 5500 system (Philips) equipped with an S12 transducer (12 MHz). M-mode images and greyscale two-dimensional parasternal short-axis images at the mid-papillary level were recorded in each rat. Measurements were made offline by a single observer in a group-blinded fashion. Left ventricular end-diastolic and end-systolic internal diameters were measured from M-mode images permitting the calculation of left ventricular fractional shortening, left ventricular end-diastolic volume, left ventricular end-systolic volume and ejection fraction. Heart rates were determined using M-mode images. All parameters represent the average of three beats.

Histology. Hearts were fixed in 4% paraformaldehyde (Thermo Fisher Scientific) for 24 h, then subsequently placed in 70% ethanol. Samples were paraffin embedded, and 5-µm-thin transverse sections of the heart were obtained. Slides were deparaffinized in CitriSolv (Thermo Fisher Scientific) for five minutes and rehydrated using an ethanol gradient. Slides were stained with Movat's pentachrome using standard procedures or antigen retrieved with citrate buffer and immunostained as below.

Immunostaining. Fixed cells or sections were washed with PBS, permeabilized with 0.1% Triton X (Sigma–Aldrich) and blocked with 5% bovine serum albumin (Sigma–Aldrich) for 2 h. Primary and secondary antibodies were applied for 1 h each, with 3×10 min PBS washes between. Antibody details are as follows: polyclonal rabbit anti-active caspase-3 (1:40; Abcam), monoclonal mouse anti-cardiac troponin T (4 µg ml^{-1}; Developmental Studies Hybridoma Bank), Alexa Fluor 488 goat anti-mouse IgG (1:500; Thermo Fisher Scientific), Alexa Fluor 488 goat anti-rabbit IgG (1:500; Thermo Fisher Scientific) and Alexa Fluor 594 goat anti-mouse IgG (1:500; Thermo Fisher Scientific). TUNEL staining was conducted using the In Situ Cell Death Detection Kit (Sigma–Aldrich). Cells and sections were counterstained with DAPI (Thermo Fisher Scientific) or Alexa Fluor 594 Conjugate Wheat Germ Agglutinin (Thermo Fisher Scientific) per the manufacturer's protocol. Sections were mounted using ProLong Gold Antifade Mountant with DAPI (Thermo Fisher Scientific). Fluorescence images were taken using the Olympus IX81 microscope and the Hamamatsu C4742-95 camera. All images were post-processed and quantified using ImageJ.

Statistics and correlation analysis. Statistical testing was performed using two-tailed *t*-tests. Bonferroni correction was used to adjust for multiple corrections. Statistical significance was determined by $P<0.05$ unless otherwise stated.

Correlation analyses were conducted between each pair of total infarct size, isoproterenol-induced arrhythmic events, cell size and ejection fraction sets of measurements using Pearson's correlation tests.

Reporting Summary. Further information on experimental design is available in the Nature Research Reporting Summary linked to this article.

Code availability. The custom computer code used in this study is available from the corresponding author upon reasonable request.

Data availability. All data supporting the findings of this study are available within the paper and its Supplementary Information. Source data are available from the corresponding author upon reasonable request.

Received: 1 June 2017; Accepted: 20 March 2018;
Published online: 23 April 2018

References

1. Stastna, M. & Van Eyk, J. E. Investigating the secretome: lessons about the cells that comprise the heart. *Circ. Cardiovasc. Genet.* **5**, o8–o18 (2012).
2. Wei, K. et al. Epicardial FSTL1 reconstitution regenerates the adult mammalian heart. *Nature* **525**, 479–485 (2015).
3. Ohno, S. et al. Systemically injected exosomes targeted to EGFR deliver antitumor microRNA to breast cancer cells. *Mol. Ther.* **21**, 185–191 (2013).
4. Raposo, G. & Stoorvogel, W. Extracellular vesicles: exosomes, microvesicles, and friends. *J. Cell Biol.* **200**, 373–383 (2013).
5. Tkach, M. & Théry, C. Communication by extracellular vesicles: where we are and where we need to go. *Cell* **164**, 1226–1232 (2016).
6. Lo Cicero, A., Stahl, P. D. & Raposo, G. Extracellular vesicles shuffling intercellular messages: for good or for bad. *Curr. Opin. Cell Biol.* **35**, 69–77 (2015).
7. Emanueli, C., Shearn, A. I. U., Angelini, G. D. & Sahoo, S. Exosomes and exosomal miRNAs in cardiovascular protection and repair. *Vasc. Pharmacol.* **71**, 24–30 (2015).
8. Stoorvogel, W. Functional transfer of microRNA by exosomes. *Blood* **119**, 646–648 (2012).
9. Olson, E. N. MicroRNAs as therapeutic targets and biomarkers of cardiovascular disease. *Sci. Transl. Med.* **6**, 239ps3 (2014).
10. Malik, Z. A. et al. Cardiac myocyte exosomes: stability, HSP60, and proteomics. *AJP Hear. Circ. Physiol.* **304**, H954–H965 (2013).
11. Stamm, C. et al. Autologous bone-marrow stem-cell transplantation for myocardial regeneration. *Lancet* **361**, 45–46 (2003).
12. Garbern, J. C. & Lee, R. T. Cardiac stem cell therapy and the promise of heart regeneration. *Cell Stem Cell* **12**, 689–698 (2013).
13. Segers, V. F. M. & Lee, R. T. Stem-cell therapy for cardiac disease. *Nature* **451**, 937–942 (2008).
14. Toma, C., Pittenger, M. F., Cahill, K. S., Byrne, B. J. & Kessler, P. D. Human mesenchymal stem cells differentiate to a cardiomyocyte phenotype in the adult murine heart. *Circulation* **105**, 93–98 (2002).
15. Vrtovec, B. et al. Effects of intracoronary CD34$^+$ stem cell transplantation in nonischemic dilated cardiomyopathy patients: 5-year follow-up. *Circ. Res.* **112**, 165–173 (2013).
16. Karantalis, V. & Hare, J. M. Use of mesenchymal stem cells for therapy of cardiac disease. *Circ. Res.* **116**, 1413–1430 (2015).
17. Godier-Furnémont, A. F. G. et al. Composite scaffold provides a cell delivery platform for cardiovascular repair. *Proc. Natl Acad. Sci. USA* **108**, 7974–7979 (2011).
18. Gallet, R. et al. Exosomes secreted by cardiosphere-derived cells reduce scarring, attenuate adverse remodelling, and improve function in acute and chronic porcine myocardial infarction. *Eur. Heart J.* **38**, 201–211 (2016).
19. Khan, M. et al. Embryonic stem cell-derived exosomes promote endogenous repair mechanisms and enhance cardiac function following myocardial infarction. *Circ. Res.* **117**, 52–64 (2015).
20. Bian, S. et al. Extracellular vesicles derived from human bone marrow mesenchymal stem cells promote angiogenesis in a rat myocardial infarction model. *J. Mol. Med.* **92**, 387–397 (2014).
21. Mackie, A. R. et al. Sonic hedgehog-modified human CD34$^+$ cells preserve cardiac function after acute myocardial infarction. *Circ. Res.* **111**, 312–321 (2012).
22. Chong, J. J. H. et al. Human embryonic-stem-cell-derived cardiomyocytes regenerate non-human primate hearts. *Nature* **510**, 273–277 (2014).

23. Laflamme, M. A. et al. Cardiomyocytes derived from human embryonic stem cells in pro-survival factors enhance function of infarcted rat hearts. *Nat. Biotechnol.* **25**, 1015–1024 (2007).
24. Lee, A. S., Tang, C., Rao, M. S., Weissman, I. L. & Wu, J. C. Tumorigenicity as a clinical hurdle for pluripotent stem cell therapies. *Nat. Med.* **19**, 998–1004 (2013).
25. Chong, J. J. H. et al. Human embryonic-stem-cell-derived cardiomyocytes regenerate non-human primate hearts. *Nature* **510**, 273–277 (2014).
26. Serpooshan, V. & Wu, S. M. Patching up broken hearts: cardiac cell therapy gets a bioengineered boost. *Cell Stem Cell* **15**, 671–673 (2014).
27. Anderson, M. E., Goldhaber, J. I., Houser, S. I., Puceat, M. & Sussman, M. A. Embryonic stem cell-derived cardiac myocytes are not ready for human trials. *Circ. Res.* **115**, 335–338 (2014).
28. Waldenström, A., Gennebäck, N., Hellman, U., Ronquist, G. & Minetti, C. Cardiomyocyte microvesicles contain DNA/RNA and convey biological messages to target cells. *PLoS ONE* **7**, e34653 (2012).
29. Garcia, N. A., Moncayo-Arlandi, J., Sepulveda, P. & Diez-Juan, A. Cardiomyocyte exosomes regulate glycolytic flux in endothelium by direct transfer of GLUT transporters and glycolytic enzymes. *Cardiovasc. Res.* **109**, 397–408 (2016).
30. Wang, X. et al. Cardiomyocytes mediate anti-angiogenesis in type 2 diabetic rats through the exosomal transfer of miR-320 into endothelial cells. *J. Mol. Cell. Cardiol.* **74**, 139–150 (2014).
31. Zhang, X. et al. Hsp20 functions as a novel cardiokine in promoting angiogenesis via activation of VEGFR2. *PLoS ONE* **7**, e32765 (2012).
32. Kishore, R. & Khan, M. More than tiny sacks: stem cell exosomes as cell-free modality for cardiac repair. *Circ. Res.* **118**, 330–343 (2016).
33. Chernyshev, V. S. et al. Size and shape characterization of hydrated and desiccated exosomes. *Anal. Bioanal. Chem.* **407**, 3285–3301 (2015).
34. Mateescu, B. et al. Obstacles and opportunities in the functional analysis of extracellular vesicle RNA—an ISEV position paper. *J. Extracell. Vesicles* **6**, 1286095 (2017).
35. Witwer, K. W. et al. Standardization of sample collection, isolation and analysis methods in extracellular vesicle research. *J. Extracell. Vesicles* **2**, 20360 (2013).
36. Love, M. I., Huber, W. & Anders, S. Moderated estimation of fold change and dispersion for RNA-Seq data with DESeq2. *Genome Biol.* **15**, 550 (2014).
37. Yang, B. et al. The muscle-specific microRNA miR-1 regulates cardiac arrhythmogenic potential by targeting GJA1 and KCNJ2. *Nat. Med.* **13**, 486–491 (2007).
38. Tian, Y. et al. A microRNA–Hippo pathway that promotes cardiomyocyte proliferation and cardiac regeneration in mice. *Sci. Transl. Med.* **7**, 279ra38 (2015).
39. Carè, A. et al. MicroRNA-133 controls cardiac hypertrophy. *Nat. Med.* **13**, 613–618 (2007).
40. Lewis, B. P. et al. Conserved seed pairing, often flanked by adenosines, indicates that thousands of human genes are microRNA targets. *Cell* **120**, 15–20 (2005).
41. Garcia, D. M. et al. Weak seed-pairing stability and high target-site abundance decrease the proficiency of lsy-6 and other microRNAs. *Nat. Struct. Mol. Biol.* **18**, 1139–1146 (2011).
42. The Gene Ontogoly Consortium. Gene Ontology Consortium: going forward. *Nucleic Acids Res.* **43**, D1049–D1056 (2015).
43. Ashburner, M. et al. Gene ontology: tool for the unification of biology. *Nat. Genet.* **25**, 25–29 (2000).
44. Wallace, D. G. & Rosenblatt, J. Collagen gel systems for sustained delivery and tissue engineering. *Adv. Drug Deliv. Rev.* **55**, 1631–1649 (2003).
45. Protze, S. I. et al. Sinoatrial node cardiomyocytes derived from human pluripotent cells function as a biological pacemaker. *Nat. Biotechnol.* **35**, 56–68 (2016).
46. Eng, G. et al. Autonomous beating rate adaptation in human stem cell-derived cardiomyocytes. *Nat. Commun.* **7**, 10312 (2016).
47. Sontag, S. et al. Modelling IRF8 deficient human hematopoiesis and dendritic cell development with engineered iPS cells. *Stem Cells* **35**, 898–908 (2017).
48. Chen, H.-S. V., Kim, C. & Mercola, M. Electrophysiological challenges of cell-based myocardial repair. *Circulation* **120**, 2496–2508 (2009).
49. Zhu, X. et al. Comprehensive toxicity and immunogenicity studies reveal minimal effects in mice following sustained dosing of extracellular vesicles derived from HEK293T cells. *J. Extracell. Vesicles* **6**, 1324730 (2017).
50. Hou, D. et al. Radiolabeled cell distribution after intramyocardial, intracoronary, and interstitial retrograde coronary venous delivery: implications for current clinical trials. *Circulation* **112**, I150–I156 (2005).
51. Seif-Naraghi, S. B. et al. Safety and efficacy of an injectable extracellular matrix hydrogel for treating myocardial infarction. *Sci. Transl. Med.* **5**, 173ra25 (2013).
52. Lang, N. et al. A blood-resistant surgical glue for minimally invasive repair of vessels and heart defects. *Sci. Transl. Med.* **6**, 218ra6 (2014).
53. Si-Tayeb, K. et al. Highly efficient generation of human hepatocyte-like cells from induced pluripotent stem cells. *Hepatology* **51**, 297–305 (2010).
54. Ibrahim, A. G.-E., Cheng, K. & Marbán, E. Exosomes as critical agents of cardiac regeneration triggered by cell therapy. *Stem Cell Rep.* **2**, 606–619 (2014).

Acknowledgements

We thank M. Moore (Memorial Sloan Kettering Cancer Center) for making the particle-tracking instrument (NanoSight) available, and S. R. Ambati and A. Saxena (Memorial Sloan Kettering Cancer Center) for technical help. We thank Q. Li for performing animal surgeries, R. Liu and L. Zaurov for assistance with animal echocardiograms, and S. Halligan for coordinating the animal work. We thank D. Teles, N. Kim and A. Pluchinksky for assistance with the experiments. We thank B. Fine for valuable discussions on the manuscript. We gratefully acknowledge funding for this work by the NIH (HL076485, EB002520, EB17103 and GM007367), NYSTEM (C028119), the NIA (F30 AG047748) and the Lisa and Mark Schwartz Program for Reversing Heart Failure.

Author contributions

B.L., B.W.L., G.D.P., S.H., P.A.S., V.K.T. and G.V.-N. designed the study. B.L., B.W.L., K.N., A.V., R.W., J.K., M.K., L.B. and K.B. performed the experiments. B.L., B.W.L. and J.M. analysed the data. B.L., B.W.L., P.A.S., V.K.T. and G.V.-N. wrote the manuscript.

Competing interests

The authors declare no competing interests.

Additional information

Supplementary information is available for this paper at https://doi.org/10.1038/s41551-018-0229-7.

Reprints and permissions information is available at www.nature.com/reprints.

Correspondence and requests for materials should be addressed to G.V.-N.

nature research

Corresponding author(s): Gordana Vunjak-Novakovic

☐ Initial submission ☐ Revised version ☒ Final submission

Life Sciences Reporting Summary

Nature Research wishes to improve the reproducibility of the work that we publish. This form is intended for publication with all accepted life science papers and provides structure for consistency and transparency in reporting. Every life science submission will use this form; some list items might not apply to an individual manuscript, but all fields must be completed for clarity.

For further information on the points included in this form, see Reporting Life Sciences Research. For further information on Nature Research policies, including our data availability policy, see Authors & Referees and the Editorial Policy Checklist.

Experimental design

1. Sample size

Describe how sample size was determined.

All sample sizes were determined on the basis of previously established literature standards. Results from initial experiments were used to inform the need for subsequent samples on the basis of the effect sizes observed.

2. Data exclusions

Describe any data exclusions.

No data were excluded.

3. Replication

Describe whether the experimental findings were reliably reproduced.

No replication attempts were unsuccessful.

4. Randomization

Describe how samples/organisms/participants were allocated into experimental groups.

In animal studies, animals were randomly allocated into groups such that as animals were added to the experiment, the numbers of animals in each group did not significantly differ. Exosome miRNA samples were randomized prior to sequencing. Samples in all other experiments were randomly allocated when possible.

5. Blinding

Describe whether the investigators were blinded to group allocation during data collection and/or analysis.

In animal studies, the surgeon was blinded to the contents of the applied patch. In subsequent analysis of echocardiography, histology and arrhythmia, the investigators were blinded to the animal group.

Note: all studies involving animals and/or human research participants must disclose whether blinding and randomization were used.

6. Statistical parameters

For all figures and tables that use statistical methods, confirm that the following items are present in relevant figure legends (or in the Methods section if additional space is needed).

n/a	Confirmed
☐	☒ The exact sample size (*n*) for each experimental group/condition, given as a discrete number and unit of measurement (animals, litters, cultures, etc.)
☐	☒ A description of how samples were collected, noting whether measurements were taken from distinct samples or whether the same sample was measured repeatedly
☐	☒ A statement indicating how many times each experiment was replicated
☐	☒ The statistical test(s) used and whether they are one- or two-sided (note: only common tests should be described solely by name; more complex techniques should be described in the Methods section)
☐	☒ A description of any assumptions or corrections, such as an adjustment for multiple comparisons
☐	☒ The test results (e.g. *P* values) given as exact values whenever possible and with confidence intervals noted
☐	☒ A clear description of statistics including central tendency (e.g. median, mean) and variation (e.g. standard deviation, interquartile range)
☐	☒ Clearly defined error bars

See the web collection on statistics for biologists for further resources and guidance.

Software

Policy information about availability of computer code

7. Software

Describe the software used to analyze the data in this study.	General data were analysed using Microsoft Excel (2016) and MATLAB(R2015a). Custom code was used to measure cardiomyocyte contractility as well as endothelial networks. miRNA sequence data were analysed using Python(3.6), miRSearch(3.0), and PANTHER(11.1).

For manuscripts utilizing custom algorithms or software that are central to the paper but not yet described in the published literature, software must be made available to editors and reviewers upon request. We strongly encourage code deposition in a community repository (e.g. GitHub). *Nature Methods* guidance for providing algorithms and software for publication provides further information on this topic.

Materials and reagents

Policy information about availability of materials

8. Materials availability

Indicate whether there are restrictions on availability of unique materials or if these materials are only available for distribution by a for-profit company.	No unique materials were used.

9. Antibodies

Describe the antibodies used and how they were validated for use in the system under study (i.e. assay and species).	Antibodies were used at the following concentrations: anti-TSG101 rabbit polyclonal antibody (1:1,000, abcam, Cambridge, UK), anti-Alix polyclonal antibody (1:8,000, Covalab, Villeurbanne, France), anti-GM130 mouse monoclonal antibody (1:500, BD Transduction Laboratories, Franklin Lakes, NJ), anti-Rab5 mouse monoclonal antibody (1:1,000, Synaptic Systems, Goettingen, Germany), polyclonal rabbit anti-active caspase 3 (1:40, Abcam, Cambridge, MA), monoclonal mouse anti-cardiac troponin T (4 µg/mL, Developmental Studies Hybridoma Bank, Iowa City, IA, Alexa Fluor 488 goat anti-mouse IgG (1:500, ThermoFisher Scientific, Waltham, MA), Alexa Fluor 488 goat anti-rabbit IgG (1:500, ThermoFisher Scientific, Waltham, MA), Alexa Fluor 594 goat anti-mouse IgG (1:500, ThermoFisher Scientific, Waltham, MA). TUNEL staining was conducted with the in situ cell death detection kit (Sigma-Aldrich, St. Louis, MO). Cells and sections were counterstained with DAPI (ThermoFisher Scientific, Waltham, MA) or Alexa Fluor 594 conjugated Wheat Germ Agglutinin (ThermoFisher Scientific, Waltham, MA) per manufacturer protocol. Sections were mounted using ProLong Gold Antifade Mountant with DAPI (ThermoFisher Scientific, Waltham, MA).

10. Eukaryotic cell lines

a. State the source of each eukaryotic cell line used.	Human iPS cell line C2A was provided through a collaboration with Stephen A. Duncan.
b. Describe the method of cell line authentication used.	The C2A cell line has been extensively characterized in a previously published article: Si-Tayeb et al., Hepatology, 2010
c. Report whether the cell lines were tested for mycoplasma contamination.	Cell lines were tested for mycoplasma contamination regularly.
d. If any of the cell lines used are listed in the database of commonly misidentified cell lines maintained by ICLAC, provide a scientific rationale for their use.	No commonly misidentified cell lines were used.

Animals and human research participants

Policy information about studies involving animals; when reporting animal research, follow the ARRIVE guidelines

11. Description of research animals

Provide details on animals and/or animal-derived materials used in the study.	Male athymic nude (Hsd:RH-Foxn1rnu) Sprague Dawley Rats (Harlan, Indianapolis, IN) age 15-19 weeks were used in this study.

Policy information about studies involving human research participants

12. Description of human research participants

Describe the covariate-relevant population characteristics of the human research participants.	The study did not involve human research participants.